Optimizing the detection of nonstationary signals by using recurrence analysis

Thiago de Lima Prado, Gustavo Zampier dos Santos Lima, Bruno Lobão-Soares, George C. do Nascimento, Gilberto Corso, John Fontenele-Araujo, Jürgen Kurths, and Sergio Roberto Lopes

Citation: Chaos **28**, 085703 (2018); doi: 10.1063/1.5022154
View online: https://doi.org/10.1063/1.5022154
View Table of Contents: http://aip.scitation.org/toc/cha/28/8
Published by the American Institute of Physics

Optimizing the detection of nonstationary signals by using recurrence analysis

Thiago de Lima Prado,[1] Gustavo Zampier dos Santos Lima,[2] Bruno Lobão-Soares,[3] George C. do Nascimento,[4] Gilberto Corso,[3] John Fontenele-Araujo,[5] Jürgen Kurths,[6,7] and Sergio Roberto Lopes[6,7,8,a)]

[1]*Instituto de Engenharia, Ciência e Tecnologia, Universidade Federal dos Vales do Jequitinhonha e Mucuri, 39.440-000 Janaúa, Brazil*
[2]*Escola de Ciências e Tecnologia, Universidade Federal do Rio Grande do Norte, 59078-970 Natal, Brazil*
[3]*Departamento de Biofísica e Farmacologia, Universidade Federal do Rio Grande do Norte, 59078-970 Natal, Brazil*
[4]*Departamento de Engenharia Biomédica,Universidade Federal do Rio Grande do Norte, 59078-970 Natal, Brazil*
[5]*Departamento de Fisiologia, Universidade Federal do Rio Grande do Norte, 59078-970 Natal, Brazil*
[6]*Potsdam Institute for Climate Impact Research, Telegraphenberg A 31, 14473 Potsdam, Germany*
[7]*Department of Physics, Humboldt University Berlin, 12489 Berlin, Germany*
[8]*Departamento de Física, Universidade Federal do Paraná, 81531-980 Curitiba, Brazil*

(Received 11 January 2018; accepted 23 April 2018; published online 24 August 2018)

Recurrence analysis and its quantifiers are strongly dependent on the evaluation of the vicinity threshold parameter, i.e., the threshold to regard two points close enough in phase space to be considered as just one. We develop a new way to optimize the evaluation of the vicinity threshold in order to assure a higher level of sensitivity to recurrence quantifiers to allow the detection of even small changes in the dynamics. It is used to promote recurrence analysis as a tool to detect nonstationary behavior of time signals or space profiles. We show that the ability to detect small changes provides information about the present status of the physical process responsible to generate the signal and offers mechanisms to predict future states. Here, a higher sensitive recurrence analysis is proposed as a precursor, a tool to predict near future states of a particular system, based on just (experimentally) obtained signals of some available variables of the system. Comparisons with traditional methods of recurrence analysis show that the optimization method developed here is more sensitive to small variations occurring in a signal. The method is applied to numerically generated time series as well as experimental data from physiology. *Published by AIP Publishing.* https://doi.org/10.1063/1.5022154

The detection of nonstationary behavior of time series or spatial patterns has a plethora of applications on all major fields of science, e.g., physics,[1,2] engineering,[1,3] and life science.[4,5] In all these areas, the breaking of the stationary condition can avoid any measure over the systems. On the other hand, a nonstationary behavior is a common feature in many situations like abrasive processes of surfaces, alterations occurring during medical monitoring of vital signals, or subtle changes in the vibrational condition of a crucial part of a satellite. These are just few examples where identifying subtle changes in time or space is a key problem. In general, the human eye cannot identify tiny changes occurring in a long sequence of data; in these cases, it is worth making use of quantifiers that can translate small changes in visibly distinct patterns. A promising framework to analyze subtle changes in data is recurrence analysis. Here, we develop an optimized way to show how recurrence quantifiers can be used as an efficient tool to detect nonstationary changes in time and space profiles.

I. INTRODUCTION

Considering a time signal as a sequence of events, a system is classified as nonstationary if a computed mean momentum of a suitable distribution function suffers changes of its value from elapsed to elapsed time, even when computed for a sufficient large but finite elapsed time.[3] A common cause of such nonstationary behavior of a signal is the unavoidable parameter changes occurring during data acquisition. Other sources of nonstationarity are system and ambient interactions, or due to the data acquisition process itself.

Almost all methods of time series analysis require some degree of stationarity of the system under investigation. In this scenario, an important question on signal analysis is how to evaluate a possible nonstationary behavior of a data acquisition process. In general, the correct identification of stationary or nonstationary responses of a system is strongly dependent on an adequate data capture. However, natural oscillations of a signal cannot be confused as a proof of nonstationarity since natural (pseudo) periods displayed by the system need to be considered. Many systems are classified as nonstationary, for example, financial markets,[6] where we know that parameters change all the time. Others are difficult to be classified since natural oscillations and drifts can be very hard to distinguish, as is the case of climate changes.[1]

Considerations about the nonstationary behavior of the dynamics due to parameter and/or environment changes during a data capture are an undesired complication. Hence, nonstationary time series is often discarded as unsuitable for analysis.[2] However, the detection of nonstationarity might actually represent an interesting aspect of the dynamics, revealing properties of the system itself.

a)lopes@fisica.ufpr.br

In order to trace nonstationarity data, studies of nonlinear systems have focused on some important questions, particularly related to: (i) the temporal organization of complex fluctuations in output signals;[7] (ii) effects of environment changes in output signals on measures derived from nonlinear analyses;[4,8] and (iii) the way to treat nonstationarity—as systems response to environment perturbations or as intrinsic characteristics of the system related to underlying control mechanisms.[5,9] A key question in nonlinear systems is how to infer parameter and/or coupling changes of systems and how they evolve in time. In this direction, several methods have been recently developed to identify and quantify forms of interactions between systems, where coupling is not *a priori* known, including the study of phase, lag, or generalized synchronizations of chaotic oscillators,[10,11] instantaneous increment cross correlation methods,[12] Bayesian-based inference,[13] and time delay stability methods to quantify coupling between diverse systems.[14,15]

Another class of methods to analyze time series and space profile are those based on recurrence properties of time series,[16–18] space profiles,[19] and 2*D* data images.[20] They can be used when the underlying mechanisms of the systems responsible to generate these data are not *a priori* known. Here, we demonstrate how the vicinity threshold parameter used as a free parameter in recurrence analyses[16,21] can be optimized and unequivocally determined to allow detection of coupling and/or parameter changes in real systems. We also show that such an optimization delivers information about a given system when only indirect captured data are available, i.e., the case for what just an output of a second system coupled to the first is accessible.

To validate our analysis, first, we apply recurrence analysis to simulated time series of paradigmatic systems subject to parameter changes and/or varying coupling coefficients. Second, we apply the same technique to experimental physiological data, recently discussed in the literature.[22] We show evidences that the success of the recurrence analysis in all situations is only possible if an optimized and individual dynamical procedure to calculate the vicinity threshold parameter is employed.

The paper is organized as follows: Sec. II gives the methodology to define the optimized vicinity threshold parameter for recurrence analysis; Sec. III applies the optimized recurrence vicinity threshold parameter to detect small changes in the parameter space by the analysis of nonlinear model systems; Sec. IV is devoted to detect weakly nonstationary behavior of experimental data; finally, Sec. V is dedicated to our discussions and conclusions.

II. RECURRENCE ANALYSIS AND THE VICINITY THRESHOLD PARAMETER

Visual analysis of embedded information and patterns in long and transient time series or in space profile discretization are complex tasks. To help the analyses in such cases, it is preferable to study simpler distribution momenta or other quantifiers obtained from the time series and able to summarize the information carried by the signal. A well recognized tool to perform this task is the recurrence analysis. The concept of recurrence comes from Henri Poincaré's work,[23] and it is a fundamental attribute of dynamical systems. However, a modern visualization method, known as recurrence plot (RP), was introduced much later.[24] The RP is a graphical tool to identify recurrence in a trajectory $\mathbf{A}_i \in \mathbb{R}^d$ phase space, $i = 1, \ldots, N$, or among two trajectories $\mathbf{A}_i$, $\mathbf{B}_i$, and it is based on the recurrence matrix[24]

$$\mathbf{R}_{ij} = \begin{cases} 1 & \text{if } ||\mathbf{A}_i - \mathbf{A}_j|| \leq \varepsilon \\ 0 & \text{if } ||\mathbf{A}_i - \mathbf{A}_j|| > \varepsilon \end{cases} \quad i,j = 1 \cdots N, \tag{1}$$

where $||\cdot||$ is an appropriate norm, ε is the vicinity threshold parameter, and N is the length of the analyzed time series. The RP is a matrix of "ones" and "zeros," where one (zero) indicates a recurrent (non-recurrent) point in phase space.

Since these plots are not easy to be used to conclude about states of the system, substantial efforts have been made to summarize their information content into recurrence quantifiers.[16,25,26] Other techniques, including measuring the dissimilarity between density distributions[27] and analysis of the loss of recurrence in time series,[2] were also proposed.

The use of recurrence quantifiers to an entire signal brings useful results. Nevertheless, large time series lengths N lead to recurrence matrices of size $N \times N$ that can be unpractical to be computed. For these cases, it is preferable to divide the whole signal into smaller time windows of size K, for $K \ll N$. For each interval, windowed computed recurrence quantifiers are captured. In this way, important features about the dynamics of a system can be obtained.[16,18,20]

An important characteristic of the RP given by Eq. (1) is the presence of vertical (horizontal) and diagonal sets of points (lines) formed from a sequence of recurrence points. Based on the recurrence matrix $\mathbf{R}_{ij}(\varepsilon)$, one can define the recurrence quantifier $[\Delta(\varepsilon)]$, measuring the ratio of all recurrence points located in diagonal lines versus all recurrence points in the RP:[16]

$$\Delta(l_{\min}, \varepsilon) = \frac{\sum_{l=l_{\min}}^{N} lP(l,\varepsilon)}{\sum_{l=1}^{N} lP(l,\varepsilon)}, \tag{2}$$

where $P(l,\varepsilon)$ is the probability distribution function of a diagonal line of $\mathbf{R}_{i,j}(\varepsilon)$ with length l, and $l_{\min}$ is the minimum number of points to be considered in a diagonal line of $\mathbf{R}_{i,j}(\varepsilon)$, i.e., the shortest diagonal line taken into account. $\Delta(l_{\min}, \varepsilon)$ is called *Determinism* but here we avoid using the traditional term since we are exploring the optimized sensitivity of the quantifier to detect subtle changes and nonstationary behavior in time series, and also to detect coupling between systems based on its time or space profile signals.

The explicit dependence on ε and $l_{\min}$ of $\Delta(l_{\min}, \varepsilon)$ in Eq. (2) indicates that adequate values of these parameters must be found before the use of the recurrence quantifier. Here, we fixed $l_{\min} = 2$ for the Lorenz and Rössler oscillators and $l_{\min} = 200$ for the experimental sleep data such that from now on, we suppress the explicit dependence on $l_{\min}$, writing $\Delta(l_{\min}, \varepsilon) = \Delta(\varepsilon)$. Considering the different pseudo-periods of each example, we have sampled the time series using appropriate time delays (τ) such that τ is much smaller than the particular pseudo-periods,[28] namely, $\tau = 50$, 150, and 1 for the Lorenz, Rössler, and the sleep time series, respectively.

On the other hand, the choice of ε is critical in order to use the quantifier as a useful tool to detect nonstationary behavior. In fact, the literature gives protocols for estimating adequate values, depending on the particular use of the recurrence quantifier.[16] Typical recommendations are to set ε values to a few percent of the maximum phase space diameter.[16] Often, a 10% of the maximum phase space diameter is used.[25] Another possibility is to choose ε according to a fixed recurrence density of the recurrence plot by seeking a scaling region in the recurrence density.[26]

However, the literature points out that all these protocols may not be suitable for non-stationary data.[16,26] For this case, it was proposed to choose smaller ε, such that the density of recurrence point stays approximately around 1%.[26] Some criteria for the choice of ε also take into account that the signal is composed of real data superposed by noise with a given standard deviation[29] such that some similar results for noise and noise-free situations can be obtained. Many statistical techniques based on recurrence produce reliable and consistent detection of nonstationarity by measuring some of the intrinsic recurrence properties of the dynamics[2,30–33] including experimental applications.[34–36] Most of these techniques are also dependent on adequate threshold parameters.

In the following, we develop a new protocol to choose appropriated ε values to deal with nonstationary data. We consider a time series of length N sampled in windows of size K, ($K \ll N$) and supposing a moving window step size of S ($S < K$) points such that $K - S$ points will be overlapping from one window to the next. The K time series lengths must contain a large number of pseudo-periods of the signal, while the S values can be chosen based on an acceptable fluctuation of the computed quantifier. In general, larger values of S lead to larger fluctuations of the quantifier. For each window i, a particular value $\Delta_i(\varepsilon)$ is computed. Repeating the process for values of ε on the domain ($0 \leq \varepsilon \leq 1$), we define the function

$$\Psi[\Delta(\varepsilon)] = \frac{S}{N-K} \sum_{i=1}^{(N-K)/S} \Delta_i(\varepsilon), \tag{3}$$

as well as its derivative $d\Psi[\Delta(\varepsilon)]/d\varepsilon$. $\Psi[\Delta(\varepsilon)]$ is a continuous function expressing how the mean value of $\Delta(\varepsilon)$ varies as a function of ε. For values of $\varepsilon \sim 0$, $\Psi[\Delta(\varepsilon)]$ will be almost zero since no recurrence points will be obtained. On the other hand, for values of $\varepsilon \sim 1$, $\Psi[\Delta(\varepsilon)]$ will reach one since all points will be recurrent. For intermediate values of ε, $\Psi[\Delta(\varepsilon)]$ describes a sigmoid-like curve and $d\Psi[\Delta(\varepsilon)]/d\varepsilon$ will display a maximum for one particular value of ε, namely, ε_{opt}, the one that reflects the maximum sensitiveness of $\Delta(\varepsilon)$ to capture small changes in the time series. For critical cases, ε can be calculated for each moving window. For the case of trajectories belonging to an attractor, the value of ε will not change due to attractor stationarity. Small changes of parameters also do not alter the value of ε significantly.

The main advantage of the method is that it can be calculated rather easily and automatically, as long as K is large enough to sample, approximately, the maximum phase space diameter. Given specific data, the method has the ability to calculate the most sensitive value of the vicinity threshold parameter. The protocol allows reliable results using small time series size and explores the maximum sensitivity of $\Delta(\varepsilon)$ to capture small changes due to the nonstationary behavior of the signals.

Using this optimal value of the vicinity threshold that gives the maximum sensitiveness of $\Delta(\varepsilon)$ to capture subtle time changes of the signal, we define the following protocol to compute $\Delta(\varepsilon)$: For a given time series $A(t)$ defined in $\mathbb{R}^1$ and length N, we calculate windowed computed $\Delta(\varepsilon)$ for $\varepsilon = \varepsilon_{\text{opt}}$ defined as $\Delta(\varepsilon_{\text{opt}})$. To do so, we divide the original time series $A(t)$ in time segments $A_i(t)$ corresponding to a time interval $[t_{(l-K)} - t_{(l)}]$ of length K points. We calculate $\Delta(\varepsilon_{\text{opt}})$ for each time segments $[t_{(l-K)} - t_{(l)}]$ and we assign the value of $\Delta(\varepsilon_{\text{opt}})$ at point t_l. So, the value of $\Delta(\varepsilon_{\text{opt}})$ computed for $t = t_l$ quantifies the dynamics of the system prior to time t_l at which $\Delta(\varepsilon_{\text{opt}})$ is positioned—i.e., variations in the signal $A(t)$ at times $t > t_l$ do not affect the calculation of $\Delta(\varepsilon_{\text{opt}})$. Since $\Delta(\varepsilon_{\text{opt}})$ is calculated for times $t < t_l$, a change in the trends of $\Delta(\varepsilon_{\text{opt}})$ prior to any changes in the data time series $A(t > t_l)$ indicates also that $\Delta(\varepsilon_{\text{opt}})$ is able to predict such variations by capturing subtle changes in the data ahead of such events, as is the case for the experimental signals studied in this paper.

Finally, in Secs. III–V, we set the embedding dimension equal to one, since in an experimental situation the dimension of the system is not known *a priori*. In spite of that, the optimization of the threshold parameter offers a way to obtain reliable results concerning the nonstationarity detection, even when a time series of just one variable or a composition of variables are used to evaluate the dynamics.

III. THE RECURRENCE QUANTIFIER AS A TOOL TO DETECT NONSTATIONARY BEHAVIOR IN DYNAMICAL SYSTEMS

To demonstrate the ability of windowed recurrence quantifier analysis associated with the use of the optimized vicinity threshold to detect nonstationary behavior of time series, we perform recurrence analysis applied to paradigmatic examples of coupled chaotic systems, two Lorenz and two Rössler oscillators.[37] The Lorenz coupled system is written as

$$\dot{x}_i = \sigma_i(y_i - x_i), \tag{4}$$

$$\dot{y}_i = x_i(\rho_i - z_i) - y_i, \tag{5}$$

$$\dot{z}_i = x_i y_i - \beta_i z_i + \gamma_{i,j}(z_j - z_i). \tag{6}$$

The Rössler coupled system is described by

$$\dot{x}_i = -y_i - z_i + \gamma_{i,j}(x_j - x_i), \tag{7}$$

$$\dot{y}_i = x_i + a_i y_i, \tag{8}$$

$$\dot{z}_i = b_i + z_i(x_i - c_i), \tag{9}$$

where $i = 1, 2$, $j = 1, 2, j \neq i$, and we set a bi-directional coupling such that the coupling coefficient $\gamma_{1,2} = \gamma_{2,1} = 0.75$ for the coupled Lorenz oscillators and $\gamma_{1,2} = \gamma_{2,1} = 0.10$ for the coupled Rössler oscillators. We choose standard parameter values for the Lorenz, $\sigma_i = 10.0$, $\rho_i = 28.0$, $\beta_i = 8/3$, $i = 1, 2$, and Rössler, $a_i = 0.2$, $b_i = 0.2$, $c_i = 14.0$, $i = 1, 2$ systems, for which both exhibit chaotic regimes. Values of the coupling parameters $\gamma_{i,j}$ are set such that both oscillators are unsynchronized.

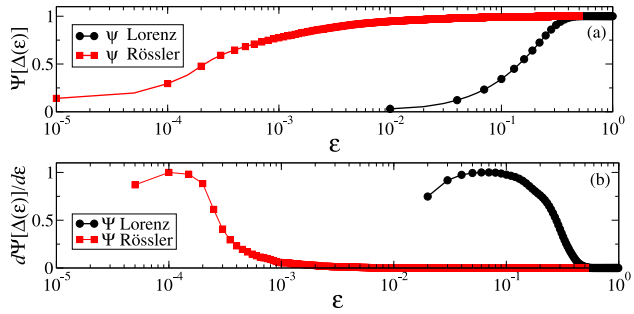

FIG. 1. (a) Optimization procedure to obtain the vicinity threshold parameter (ε) for the Lorenz and Rössler systems. The optimized value for ε is obtained considering the maximum variation of the function $\Psi[\Delta(\varepsilon)]$ as a function of ε. (b) Normalized values for $d\Psi[\Delta(\varepsilon)]/d\varepsilon$ to better identify the value of the ε of maximum variation of $\Psi[\Delta(\varepsilon)]$. Observe the large interval of possible values of the vicinity threshold parameter ε.

Figure 1(a) depicts our results for the function $\Psi[\Delta(\varepsilon)]$ given by Eq. (3) and applied to two different signals obtained from the Lorenz and Rössler oscillators. For the Lorenz system, we choose to use a composition of all components of the trajectory in the $d = 3$ phase space such that we set $A(t) = \sqrt{x_2^2(t) + y_2^2(t) + z_2^2(t)}$ defined in $\mathbb{R}^1$ and for the Rössler system just the component $y_2(t)$ is used, such that in this case $A(t) = y_2(t)$, exemplifying a situation where just one component of the state vector is available. Other combinations or variables can also be used. Figure 1(b) shows $d\Psi[\Delta(\varepsilon)]/d\varepsilon$ normalized by its maximum to evidence better the value of ε_{opt} for which the maximum sensitivity of $\Delta(\varepsilon)$ is acquired. Here, we have used $S = 80$, $K = 8 \times 10^3$, and $N = 3.6 \times 10^5$ for all simulations. The sigmoid characteristic for $\Psi[\Delta(\varepsilon)]$ is clear. Both lines in Fig. 1(a) give us a well defined optimum value for ε, namely, the one for which $d\Psi[\Delta(\varepsilon)]/d\varepsilon$ displays a maximum of the corresponding curves in Fig. 1(b). Observe that, despite the common sigmoid shape of $\Psi[\Delta(\varepsilon)]$, the values of ε for which $d\Psi[\Delta(\varepsilon)]/d\varepsilon$ reaches its maximum vary in a large interval of ε. Similar dynamical systems as is the case of the Lorenz and Rössler oscillators lead to very different values of the optimum ε, namely, ≈ 0.1 for the Lorenz system and ≈ 0.00016 for the Rössler system.

The reason for such a large difference in the values of ε_{opt} reflects the fact that the Rössler dynamics develops almost in a plane, but is subjected to ejections, leading the system to present two distinct time and spatial scales. Small values of ε need to be used in order to capture small differences in the planar dynamics. Our automatic method to select the vicinity threshold parameter captures this special characteristic of the dynamics, setting the correct optimized value of ε.

To study nonstationary properties of the systems, time series of length 3.6×10^5 was numerically computed for both oscillators discarding a transient time of 3.0×10^4. At time $t_{\text{half}} = t_{\text{end}}/2 = 1.8 \times 10^5$, the parameters $\rho_1 = 28.0$ and $c_1 = 14.0$ (just for one of each coupled oscillators) are linearly increased in time along 4000 time units, until $\rho_1 = 29.0$ and $c_1 = 14.5$. The changes of the parameters are subtle enough and result in no visible effects in the time series output of both coupled oscillators, especially on the coupled oscillators which do not contain direct changes on the parameters as can be observed in Fig. 2.

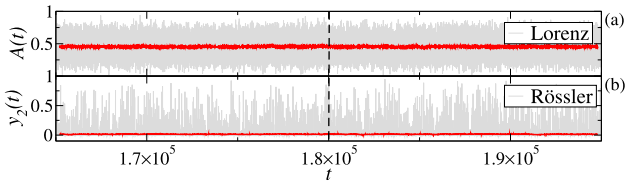

FIG. 2. Time series of $A(t) = \sqrt{x_2^2(t) + y_2^2(t) + z_2^2(t)}$ for Lorenz and $y_2(t)$ for the Rössler oscillators, sampling the time interval for which the parameters of both systems suffer changes, imposing a nonstationary behavior. The changes are not visible in the time series, neither in a smooth running average (size 100) of the signal (red curve). The vertical dashed line marks the time for which parameters $\rho_1 = 28.0$ and $c_1 = 14.0$ are linearly increased in time along 4000 time units, until $\rho_1 = 29.0$ and $c_1 = 14.5$.

To test the sensitivity of the recurrence quantifier $\Delta(\varepsilon)$ to capture the imposed nonstationarities, Fig. 3 displays results for the values of $\Delta(\varepsilon)$ for both systems, Lorenz [panels (a)–(c)] and Rössler [panels (d)–(f)], respectively, making use of the recurrence quantifier $\Delta(\varepsilon)$ associated with 3 different ways to compute the vicinity threshold parameter ε. Since only relative changes of $\Delta(\varepsilon)$ are important to quantify the nonstationary behavior, each $\Delta(\varepsilon)$ can be normalized by the relations

$$\Delta'(\varepsilon) = \Delta(\varepsilon) - \min[\Delta(\varepsilon)], \tag{10}$$

$$\Delta''(\varepsilon) = \Delta'(\varepsilon)/\max[\Delta'(\varepsilon)]. \tag{11}$$

The protocol maximizes all changes occurring in the time series obtained for the windowed $\Delta''(\varepsilon)$. From now on, we simplify the notation suppressing the double quote on $\Delta(\varepsilon)$ for all $\Delta(\varepsilon)$ computed here. In the ideal case, the distribution of a specific $\Delta(\varepsilon)$ is able to characterize the nonstationarity imposed by a parameter change (or other nonstationary imposed to the system) since the analysis protocol will make $\Delta(\varepsilon)$ values map to only one of the possible intervals, (0.0, 0.5) or (0.5, 1.0) for t before the parameter changes, shifting to the opposite interval for t after the parameter change.

Panels (a) and (d) of Fig. 3 depict results of the traditional method to choose the vicinity threshold parameter as 10% of the domain of the data for the Lorenz and Rössler systems. For the Lorenz system, this procedure is revealed to be adequate since after the stationarity breaking imposed in $t = t_{\text{half}}$ the quantifier starts to map the opposite interval of values. On the other hand, the same procedure results in being inefficient for the Rössler system.

Panels (b) and (e) of Fig. 3 show results for $\Delta(\varepsilon)$ using a fluctuating vicinity threshold parameter but a constant recurrence density rate, set to be approximately 0.01 (1% of recurrence points) for each moving window. Despite the high computational cost to compute a constant recurrence rate for each window, this procedure results in being only marginally efficient. For both cases, the running average of the quantifier values oscillates around the frontier between the two intervals of mapped values.

The optimized procedure to obtain the vicinity threshold parameter determined by the function $\Psi[\Delta(\varepsilon)]$ given in Eq. (3) and plotted in Fig. 1 is employed in Fig. 3, panels (c) and (f). Observe that we obtain very different values for the vicinity threshold parameter for each system. While for

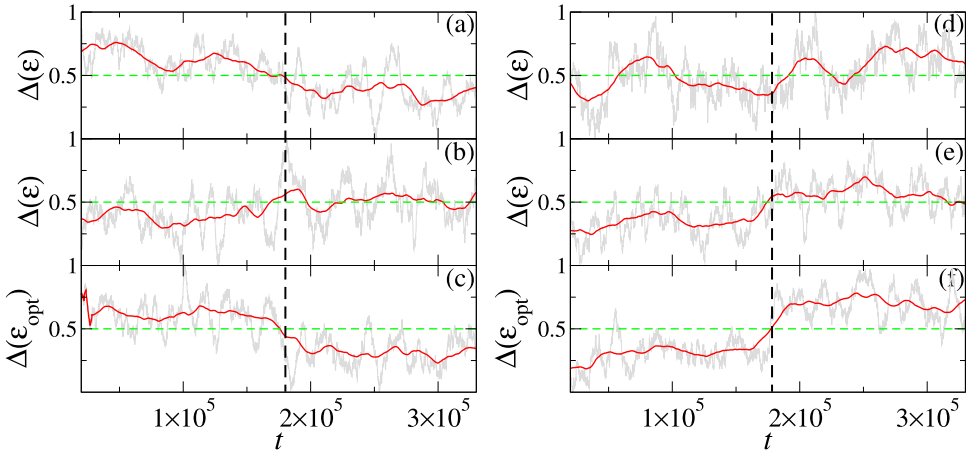

FIG. 3. Windowed computed values of $\Delta(\varepsilon)$ applied to the Lorenz [panels (a)–(c)] and Rössler [panels (d)–(f)] systems. In panels (a) and (d), a fixed size (10% of the phase space) for the vicinity threshold parameter is employed. In panels (b) and (e), a fixed density of recurrence points is used. In panels (c) and (f), optimized values obtained by $\Psi[\Delta(\varepsilon)]$, Eq. (3), are applied. The green dashed line marks the limit of oscillation for both stationary regimes, (0.0, 0.5) and (0.5, 1.0), that should be (uniquely) mapped before or after the parameter changes. The vertical dashed line sets the time for which the perturbations on ρ_1 and c_1 start.

the Lorenz oscillator the optimized procedure to compute the vicinity threshold leads to a value around $\varepsilon = 0.1$, which in fact represents 10% of the normalized domain; for the Rössler oscillator case the same procedure leads to a threshold value much smaller, $\varepsilon = 0.00016$. Despite the difference among the values of the employed vicinity threshold parameter, the methodology works adequately in both cases, as observed in Fig. 3 panels (c) and (f). Clearly, the computed values for $\Delta(\varepsilon)$ map the two different intervals of $\Delta(\varepsilon)$ before and after the changes of the system parameters.

All results displayed in Fig. 3 are obtained by using just one time series. It is important to demonstrate how the sensitivity of the method can be explored in an experimental situation, where the use of a large set of time series is not possible in general. On the other hand, to show explicitly some statistical properties of the method, Fig. 4 depicts the mean values of $\Delta(\varepsilon)$ for 30 distinct time series events. The black thick curves display the mean values while the gray regions depict the standard deviation of the mean. Observe that the optimization method (panels c and f) assures (almost) the non-overlapping of values before and after the changes of parameters. Fixed size threshold parameter [panels (a) and (c)] and fixed recurrence rate [panels (b) and (e)] methods show also better results compared to just one time series, but in these cases there exist a consistent overlapping of values before and after the imposed nonstationarity.

The dynamical changes due to the subtle increase of ρ_1 and c_1 parameters are also hardly captured by traditional momenta of the distribution function of $A(t)$ as defined for both systems. Figures 5(a)–5(h) depict normalized results of windowed computed mean $\{[A(t)]\}$, variance $\{\sigma\,[A(t)]\}$, skewness $\{s\,[A(t)]\}$, and kurtosis $\{\kappa\,[A(t)]\}$ values (gray lines) using a window size of $K = 8000$ points. To compute the momenta, we have used time series of both oscillators that have their parameters kept constant. The thick red lines superposed to the original signals observed in Figs. 5(a)–5(h) are running averages of size 400 points, just to smooth short term oscillations of the computed momenta. As seen, for the Lorenz data, Figs. 5(a)–5(d), just the variance (panel b) captures some useful information about the nonstationary properties of the systems. For the Rössler case, Figs. 5(e)–5(h), none of the momenta captures the nonstationarity imposed to data at t_{half}.

Both Lorenz and Rössler oscillators are commonly used as examples of low dimensional nonlinear chaotic systems. Nevertheless, they have quite different dynamics properties. In fact, due to the ejections from its almost planar dynamics, the Rössler oscillator displays two very distinct spatial scales. In such cases, the computation of the vicinity threshold parameter needs to take this property into account, setting a value small enough to capture changes occurring in the smallest spatial scale dynamics. Another important characteristic is related to the fact that while the Lorenz system has a maximum Lyapunov exponent around $\lambda_{\text{Lorenz}} \approx 1.5$, the Rössler oscillator has a much smaller one, $\lambda_{\text{Rössler}} \approx 0.1$. Differences in the local divergences between trajectories are important in recurrence analysis and directly related to the concept of

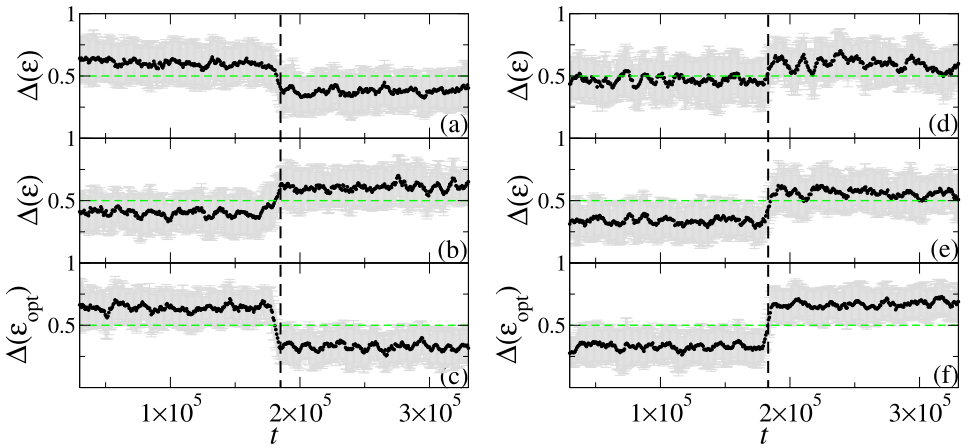

FIG. 4. Same results of Fig. 3, but now plotting mean values of the quantifiers over 30 distinct time series running (black curves). The gray areas depict the standard deviation of the mean value obtained for each time.

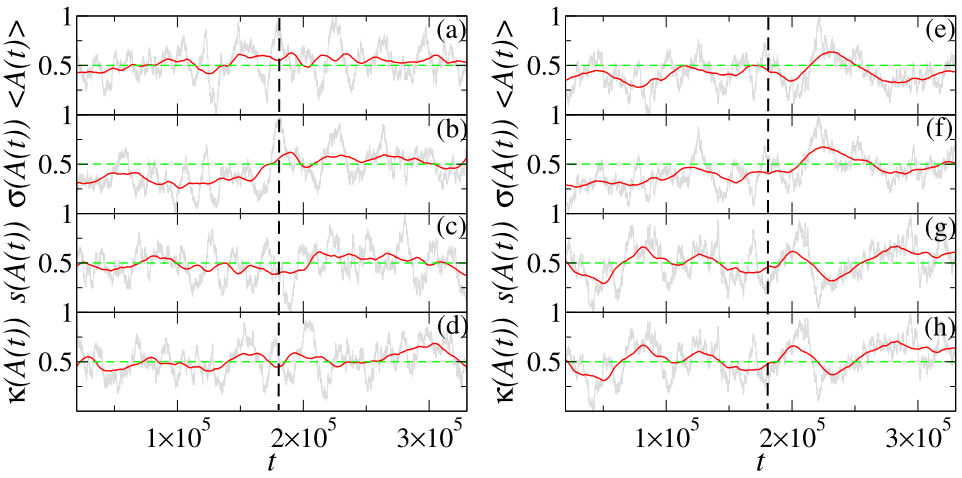

FIG. 5. Windowed statistical momenta computed from the time series of $A(t)$ of Lorenz [panels (a)–(d)] and Rössler [panels (e)–(h)] coupled oscillators. At $t = 1.8 \times 10^5$, the parameters $\rho_1 = 28.0$ and $c_1 = 14.0$ for one of each coupled oscillators are linearly increased in time along 4000 time units, until $\rho_1 = 29.0$ and $c_1 = 14.5$. Panels (a) and (e) depict the mean values, (b) and (f) the variance, (c) and (g) the skewness and (d), and (h) the kurtosis. The green dashed line marks the limit of oscillation for both stationary regimes, (0.0, 0.5) and (0.5, 1.0) that should be (uniquely) mapped before or after the parameter change. The vertical dashed line sets the time for which the perturbations on ρ_1 and c_1 start.

determinism and also an important parameter to choose the vicinity parameter. The results show that a real time evaluation of optimized vicinity threshold values can be a necessary pre-condition to adequately use recurrence quantifier analysis of data as a sensitive nonstationary measure.

Since all measures obtained for both systems have been done in oscillators that have not suffered parameter changes, the method proposed here is also effective to infer coupling between systems. It is clear that changes in one of the oscillators reflect in the space recurrence of the other. Theoretically, it seems to be a trivial question, whereas changes in one element of the coupled system cause changes in the other. But the results emphasize the necessity of an optimized method to compute the vicinity threshold parameter to obtain success in the detection of the coupling. More than that, a real time observation of changes in the parameter space and/or couplings between systems are relevant questions in practical situations. In these cases, the development of high sensitive methods to infer about nonstationary behavior turn to be an indispensable task.

IV. THE RECURRENCE QUANTIFIER AS A TOOL TO DETECT NONSTATIONARY BEHAVIOR IN EXPERIMENTAL DATA

In this section, we employ the same technique explored in Sec. III to analyze experimental data. The signals are characterized as nonstationary and composed of two synchronously physiologic records from mice sleep periods:[22,38] (i) a noninvasive accelerometer sensor signal (actiographic records) (A_{cc}) and (ii) a signal of surgery implanted intra cranial local field potential (LFP) probes (H_{pp}) capturing the electrophysiological activity of the hippocampus CA_1 brain area.[22] Both signals are recorded with a time resolution of 0.001 s continuously recorded over a 24 h period during sleep episodes of five adult mice.[22,38] We select from recordings data sets of length of 200 000 points, corresponding to 200 s of recording sleep periods and containing at least one so called arousal event, characterized here as short time periods of activity during sleep.

In this experimental setup, interesting nonstationary data emerge from Local Field Potentials of Brain hippocampus signals (H_{pp}) and also from the accelerometer signals (A_{cc}). Both data capture details of deep sleep phases, characterized (in general) by periods of inactivity interrupted by short intervals of activity called arousals.[39] In a broad sense, arousals are characterized as short temporary intrusions of wakefulness into sleep. Many characteristics of arousals have being observed, but its role in sleep is not completely understood.[39]

According to the traditional conceptual framework of the American Sleep Disorders Association criteria, "arousals are a marker of sleep disruption representing a detrimental and harmful feature for sleep." However, recent results suggest that arousals can be interpreted as an inherent part of the sleep and associated to the regulation of the sleep process itself.[22,39,40]

In this scenario, an important source of information about sleep phases properties and its interactions with arousals can be extracted from the analysis of nonstationary properties of output signals of the brain activity. One important question is how continuous variations observed in an experimental time series can be related to a nonstationary behavior of the system responsible for the data generation. In particular for the mice sleep situation, the interplay between sleep phases and arousal activities can be quantified.[22] Representative nonstationary signals of accelerometer (A_{cc}) and hippocampus (H_{pp}) data, obtained during deep sleep periods of mice for two individuals, are depicted in Figs. 7 and 8, panels (a) and (c), respectively.

A. Experimental setup

Five adult male mice were implanted with 16 chronic electrodes in the hippocampus, motor and somatosensory cortex for intracranial local field potential (LFP) recordings to characterize wake-sleep cycles. A noninvasive accelerometer with X, Y, and Z axes orientation sensor (ADXL330, Analog Devices) was associated to the head-stage of each individual. The LFP and accelerometer signals were obtained at 1 kHz sample rate. The mice data collection was performed at the Instituto Internacional de Neurociencias Edmond and Lily Safra (IINN-ELS). All animals were provided by the IINN—ELS Central Biotherium. Housing, surgical, and behavioral procedures were in accordance with the National Institutes of Health guidelines and the IINN—ELS Ethics

Committee (protocol number 08/2010) in Animal Experimentation.

We defined here an arousal as a fluctuation of the accelerometer signal that has a minimal duration of 0.3 s and an amplitude of at least three times the standard-deviation of the signal background. Arousals were selected from the slow wave sleep (SWS) cluster of state maps. The SWS records present large-amplitude slow hippocampal rhythms and low amplitude ones in the accelerometer records. The identification of deep slow wave sleep (SWS) episodes, wake, and paradoxical sleep/rapid eyes movement (REM) is made through spectral analysis using the Plexon system and LFP channel processing.[15,22,38]

B. Data treatment

The accelerometer output consists of three components of the acceleration vector $\mathbf{a} = (a_x, a_y, a_z)$. Mathematical analyses are done combining the vector components in a single vector module, at the same time that it is extracted the average of each vector component. The module of the new $\mathbf{a}$ vector formed from the components of $\mathbf{a}(i)$ is defined as $A(t) = \mathrm{A_{cc}} = \sqrt{(a_x - \hat{a}_x)^2 + (a_y - \hat{a}_y)^2 + (a_z - \hat{a}_z)^2}$, where $\hat{a}_{x,y,z}$ is the mean value of $a_{x,y,z}$.[22] For the electric hippocampus signal, the LFP is set as the signal to be analyzed such that $A(t) = \mathrm{H_{pp}}$ in this case.

C. Nonstationary sleep signals

Similarly to the case of the Lorenz and Rössler oscillators, Fig. 6(a) depicts the function $\Psi[\Delta(\varepsilon)]$ given by Eq. (3) and computed for both experimental signals, $\mathrm{A_{cc}}$ and $\mathrm{H_{pp}}$. Here, we have used $S = 80$, $K = 8 \times 10^3$, $N = 2.0 \times 10^5$, and no time delay ($\tau = 1$) is used such that all consecutive points in time series are used for all computed Δ. Again the sigmoid like curve is clear and the optimized values of the vicinity threshold parameter are set as the one for which $d\Psi[\Delta(\varepsilon)]/d\varepsilon$ displays the maximum for each signal as shown in Fig. 6(b).

To demonstrate the usefulness of the optimized vicinity threshold $\Psi[\Delta(\varepsilon)]$ computed by Eq. (3) and depicted in Fig. 6, we compute the recurrence quantifier $\Delta(\varepsilon)$ for both $\mathrm{A_{cc}}$ and $\mathrm{H_{pp}}$ data. The main objective is to characterize sleep phases as well as to suggest possible couplings among brain areas during sleep periods in mice.

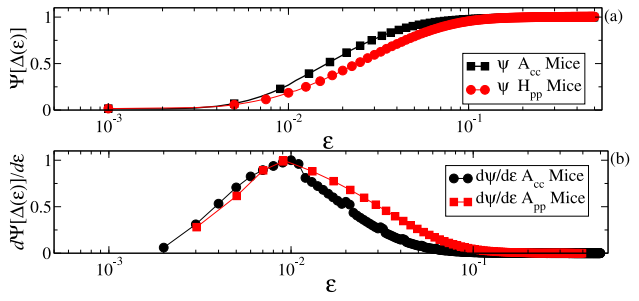

FIG. 6. (a) Optimization procedure to obtain the vicinity threshold parameter, ε, for $\mathrm{A_{cc}}$ and $\mathrm{H_{pp}}$ signals. The optimized value for ε is obtained considering the maximum variation of the function $\Psi[\Delta(\varepsilon)]$ as a function of ε. (b) Normalized values for $d\Psi[\Delta(\varepsilon)]/d\varepsilon$ to better identify the value of the ε of maximum variation of $\Psi[\Delta(\varepsilon)]$.

Based on the data obtained from all 5 individuals, we define a temporal pattern for the quantifier $\Delta(\varepsilon)$ that is representative for the transition from deep sleep to an arousal event: We say that an arousal event is likely to happen if the normalized signal $\Delta(\varepsilon)$ displays a stationary value greater than 75% of its maximum, suddenly, dropping to a value smaller than 25% of its maximum and occurring synchronously with similar changes in the hippocampus activity.[22] Examples of this scenario are depicted in Figs. 7 and 8 as gray highlighted areas. The observed behavior is a common feature during all collected data and reveals to be a robust marker to predict an arousal.[22]

Panels (a) and (c) of Figure 7 display typical time series for $\mathrm{A_{cc}}$ and $\mathrm{H_{pp}}$ signals of one individual. Bursts related to arousals in the $\mathrm{A_{cc}}$ signal are, deliberately, out of scale to provide a better view of the diffusive characteristic of the signal during inter-burst periods. Common features of the signals are the detection of changes in the mobile activity in the $\mathrm{A_{cc}}$ data and, the somewhat classical, large amplitude oscillations in the hippocampus signal during sleep.[39] The relative changes in the amplitude of the $\mathrm{H_{pp}}$ signal during the period of arousal are also observable since the increase of the (desynchronized)

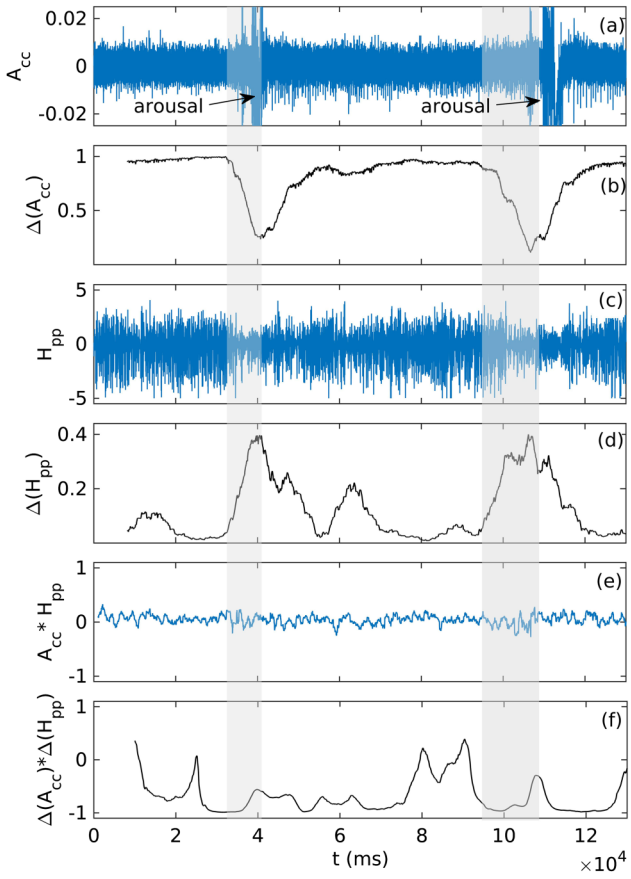

FIG. 7. Panels (a) and (c) depict typical time series for $\mathrm{A_{cc}}$ and $\mathrm{H_{pp}}$ signals displaying two arousal events (signal bursts). Panels (b) and (d) show the signature (a pattern) of $\Delta(\mathrm{A_{cc}})$ and $\Delta(\mathrm{H_{pp}})$ signals for the period between two consecutive bursts (arousals). Highlighted gray areas show time intervals just before arousal events. $\Delta(\mathrm{A_{cc}})$ starts to drop (almost) synchronously with changes in the behavior of $\mathrm{H_{pp}}$ signal, also corroborated by the growing of $\Delta(\mathrm{H_{pp}})$ and pointing to a possible coupling between $\mathrm{A_{cc}}$ and $\mathrm{H_{pp}}$ signals. Panels (e) and (f) display the windowed cross correlation between $\mathrm{A_{cc}}$ and $\mathrm{H_{pp}}$ and between $\Delta(\mathrm{A_{cc}})$ and $\Delta(\mathrm{H_{pp}})$, respectively.

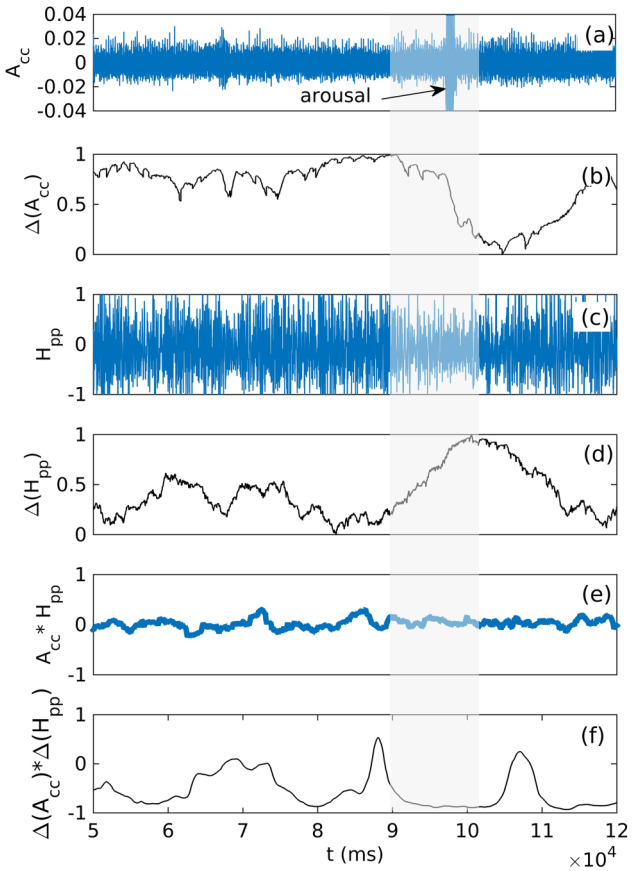

FIG. 8. Panels (a) and (c) depict typical time series for A_{cc} and H_{pp} signals before and during one burst event (arousal events). Panels (b) and (d) show the signature (pattern) of $\Delta(A_{cc})$ and $\Delta(H_{pp})$ signals for the period before the burst (arousals). The highlighted gray area shows the time interval just before an arousal event. $\Delta(A_{cc})$ starts to drop (almost) synchronously with changes in the behavior of H_{pp} signal, also corroborated by the growing of $\Delta(H_{pp})$, pointing to a coupling between A_{cc} and H_{pp} signals. Panels (e) and (f) display the windowed cross correlation between A_{cc} and H_{pp} and between $\Delta(A_{cc})$ and $\Delta(H_{pp})$, respectively.

activity of the hippocampus leads to a more incoherent, and smaller amplitude signal in the mean field collected by the LFP electrodes. Panels (b) and (d) of Fig. 7 display results for the windowed (size $K = 8192$, $S = 80$ and no delay τ) computed normalized recurrence quantifier $\Delta(\varepsilon_{opt})$ applied to the A_{cc} and $\Delta(\varepsilon_{opt})$ applied to the H_{pp} that we call simply $\Delta(A_{cc})$ and $\Delta(H_{pp})$, respectively.

An important observation is the almost stationary behavior that occurs near the saturation level of $\Delta(A_{cc})$ during periods of sleep. This saturation level is due to our procedure to capture the optimized neighborhood parameter (ε) already described in this paper, allowing a high sensitivity to capture small changes occurring during these sleep periods. Accordingly, the signal for $\Delta(H_{pp})$ during the same period stays in low levels since H_{pp} displays relatively larger oscillations during sleep, thanks to the increasing synchronization of the hippocampus activity occurring during sleep periods.

Highlighted gray areas in Fig. 7 show the characteristic pattern displayed by the windowed computed $\Delta(A_{cc})$. Such patterns occur some seconds before burst events take place. The high sensitivity of windowed computed $\Delta(A_{cc})$, thanks to our optimized method to choose ε, promotes a decrease of the magnitude of $\Delta(A_{cc})$ [Fig. 7(b)] and occurs synchronously with the growing of $\Delta(H_{pp})$ [Fig. 7(d)]. On the other hand, no clear pattern variation in A_{cc} [Fig. 7(a)] signal, even in a magnified version of time series or in the spectrogram, is observed. It is clear in this scenario that changes in the activity of the hippocampus [observable in Fig. 7(c)] also precede the effective burst in the accelerometer signal [7(a)] and are synchronized with changes in the behavior of $\Delta(A_{cc})$. At first sight, the absence of a correlation between A_{cc} and H_{pp} is inferred from Fig. 7(e) that displays low values for the windowed cross correlation of both signals for almost the entire time interval. Nevertheless, we observe that the signals for $\Delta(A_{cc})$ [Fig. 7(b)] and $\Delta(H_{pp})$ [Fig. 7(d)] display an almost complete (anti) correlation for a large percentage of the time interval, as evidenced by Fig. 7(f) that depicts the windowed cross correlation for both $\Delta(A_{cc})$ and $\Delta(H_{pp})$ signals. Observe that the strong (anti)correlated signals that reaches -1 some seconds before $\Delta(A_{cc})$ starts to drop synchronously with the increases of $\Delta(H_{pp})$. In this case, additionally to the nonstationary behavior of the time series, a possible coupling between the original A_{cc} and H_{pp} signals can be supposed. We argue that using the pattern in the recurrence quantifier $\Delta(\varepsilon)$, in principle, at least some hippocampus changes can be monitored using just analyses of noninvasive A_{cc} signals.

Since the A_{cc} and H_{pp} signals are not driven by any external common system, the (anti)correlation between $\Delta(A_{cc})$ and $\Delta(H_{pp})$ occurring in more than 80% (see Table I) of the analyzed cases suggests a coupling between both signals in general situations.[22]

Considering that A_{cc} sensors are not sensitive to any influence of the electric signal obtained by the hippocampus electrodes, a possible *cause-effect* is identified in our analysis. In this situation, we should observe the muscle movement simultaneously with activity of hippocampus since following the American Sleep Disorders Association criteria, arousals are characterized as (external) sleep disruptions. However, we observe that the hippocampus plays a role before the effective muscle activity, suggesting an internal brain coupling that breaks the stationarity of A_{cc}.[22] These results are in agreement with previous results[22] and should be further explored.

The behavior observed in the A_{cc} and H_{pp} signals, as well as in $\Delta(A_{cc})$ and $\Delta(H_{pp})$ shown in Figs. 7(a)–7(d), is general and observed in all mice sleep periods we have analyzed. Figure 8 depicts another example of all characteristics of A_{cc}, H_{pp}, $\Delta(A_{cc})$, and $\Delta(H_{pp})$ signals captured for a second individual. All main features already observed and described in Fig. 7 are also found here.

To better visualize the arousal events, Fig. 9 depicts data of a third mouse detailing 20 s of the data. Panel (a) depicts signals of A_{cc} (blue line) and H_{pp} (red line) just before and during an arousal event. Details of the oscillatory behavior

TABLE I. Summary of 221 burst events analyzed using $\Delta(A_{cc})$.

	Mice				
Diagnostic	1	2	3	4	5
$\Delta(A_{cc})$ success	94%	88%	91%	88%	71%
Precursor time (s)	4.0 ± 2.8	4.7 ± 4.0	3.2 ± 2.3	4.9 ± 4.0	5.1 ± 4.8

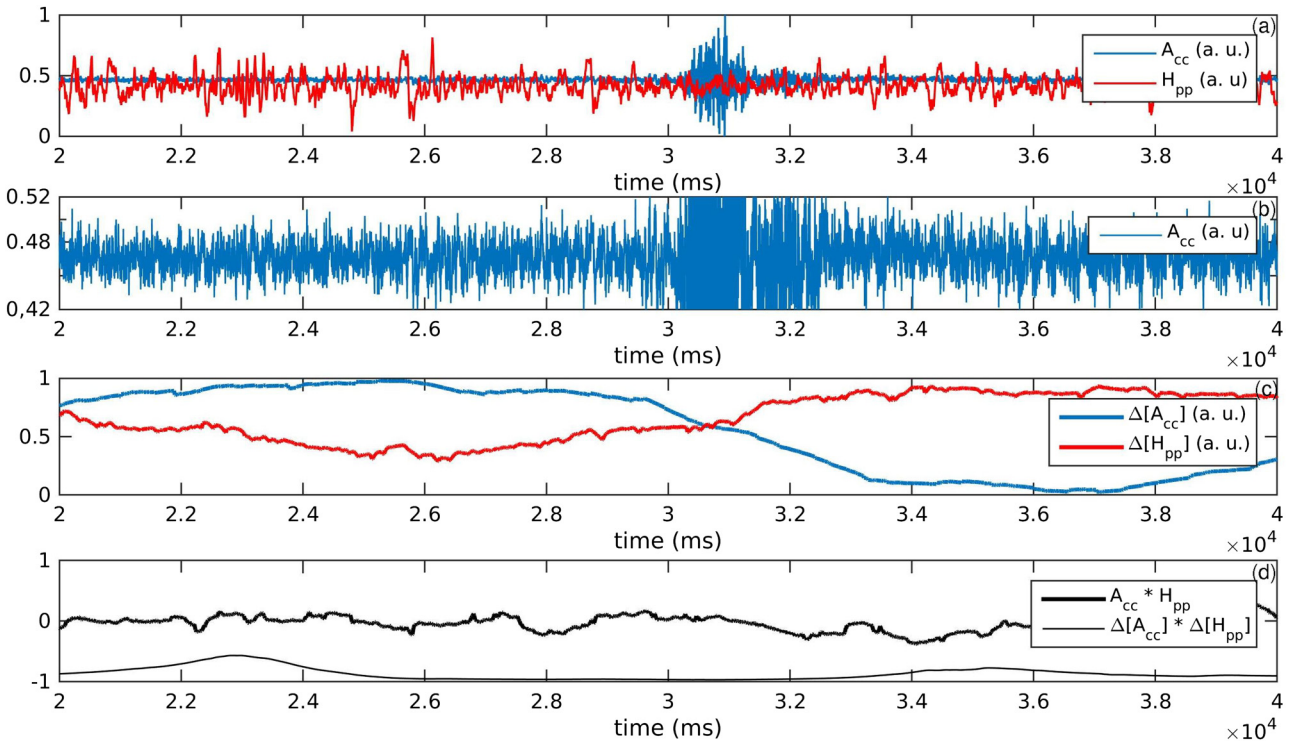

FIG. 9. Panel (a) shows details for A_{cc} (blue curve) and H_{pp} (red curve) for a short time interval just before and during the arousal; panel (b) depicts the magnification of the y scale of A_{cc} ; panel (c) displays $\Delta(A_{cc})$, (blue curves) and $\Delta(H_{pp})$ (red curve) characterizing the time period before the arousal, while in panel (d) the windowed cross correlations between A_{cc} and H_{pp} (thick curve), $\Delta(A_{cc})$, and $\Delta(H_{pp})$ (solid thin curve), are shown.

of A_{cc} during the time interval are depicted in Fig. 9(b), where a magnified y scale of panel (a) is used and the H_{pp} signal is suppressed. Figure 9(c) displays windowed (size $K = 8192$, $S = 80$ and no delay τ) computed $\Delta(A_{cc})$ (blue line) and $\Delta(H_{pp})$ (red line). Approximately at $t = 2.6 \times 10^4$ ms, both signals change its tendency, $\Delta(A_{cc})$ starts to drop at the same time that $\Delta(H_{pp})$ starts to grow. Figure 9(d) shows the windowed cross correlations for A_{cc} and H_{pp} and for $\Delta(A_{cc})$ and $\Delta(A_{cc})$. A perfect (anti)synchrony among both signals is observed in the time interval before and during the arousal event, reflecting an (almost) unitary cross correlation between $\Delta(A_{cc})$ and $\Delta(H_{pp})$. Once again no correlation between the original signals A_{cc} and H_{pp} is observed.

Taking into account the dispersion of the values of the precursor time intervals for each individual (see Table I), the same behaviors of $\Delta(A_{cc})$ and $\Delta(H_{pp})$ are found in all analyzed mice and for the majority of events. The signals for all individuals display a clear pattern in the recurrence quantifier $\Delta(\varepsilon)$, namely, $\Delta(\varepsilon)$ from A_{cc} data starts to drop some seconds before any visual evidences of arousal, but at the same time that H_{pp} signal also changes. We believe that the synchronism among both signals is associated to a coupling between the hippocampus brain area and the cortex region responsible for mice motor activities.

Table I summarizes the statistical robustness of the results discussed until now. Considering all 221 burst events dealt within the experiment, a $\Delta(A_{cc})$ success in Table I means the percentage of arousal events for which the signature in $\Delta(A_{cc})$ correctly predicts an arousal event. The precursor time is the time interval for which the $\Delta(A_{cc})$ signal starts to drop before any movement being observed in the individuals behavior. As observed, the $\Delta(A_{cc})$ pattern occurs in a great majority of arousal events. Such high occurrence of similar pattern in the $\Delta(A_{cc})$ signal before arousals suggests that the procedure developed here can be used as an efficient tool in studies related to sleep. The data analysis brings a serious question to be investigated, namely, the possibility to infer about changes in the internal hippocampus activity by making use only of the $\Delta(A_{cc})$ noninvasive signal.

The results obtained so far are due to the optimized method to compute the individualized vicinity threshold parameter for each time series. The same analysis can be done using a more traditional fixed size threshold parameter $\varepsilon = 10\%$ of the phase space, without distinction of time series. Explicit comparisons of a fixed $\varepsilon = 10\%$ of the phase space versus the analyses presented in Figs. 7 and 8, panels (b) and (d) are depicted in Fig. 10. Figure 10(a) shows that for this particular case, the vicinity threshold computed as 10% of the phase space and applied to the A_{cc} signal saturates $\Delta(A_{cc})$ during the diffusive part of the data (when no arousals are observed). The smooth decrease of $\Delta(A_{cc})$ observed some seconds before the arousal and highlighted as gray areas to characterize the time interval just before an arousal is not clearly shown. Also, the progressive recovery of $\Delta(A_{cc})$ after the arousal is not revealed either. The signals for $\Delta(A_{cc})$ [panels (a)] and $\Delta(H_{pp})$ [panel (b)] do not correlate with each other, as they are when optimized values of ε are used. Figures 10(c) and 10(d) compare the behavior for another individual, originally depicted in Figs. 8(b) and 8(d). Here, the diffusive part of the signal is adequately captured, but again the smooth decrease occurring few seconds before the arousal and the recovery of the $\Delta(A_{cc})$ for the time interval

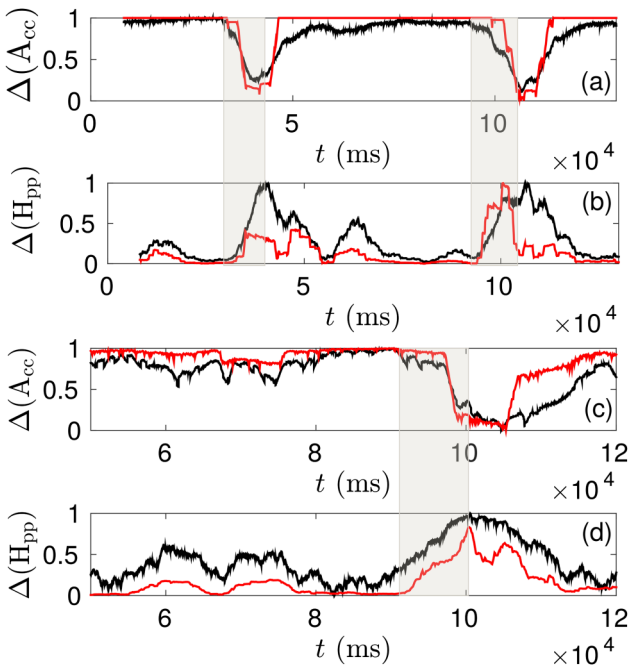

FIG. 10. Explicit comparison of the characterizations of sleep phase of mice using recurrence analysis for optimized vicinity threshold parameter (black curves) and using a standard value of 10% of the phase space (red curves). Highlighted areas represent the time intervals before arousals, where the quantifier $\Delta(\varepsilon)$ using optimized vicinity threshold is able to capture precursor changes in the signal.

after the arousal is not observed. For this case, the properties of the H_{pp} signal are captured almost correctly, but again a correlation between $\Delta(A_{cc})$ and $\Delta(H_{pp})$ is not observed.

Figure 10 makes clear that, despite data similarity, the recurrence properties of both signals only reveal their proper characteristics if an adequate vicinity parameter is individually computed. Similar comparisons can be done using other recurrence methods. The possibility to evaluate in real time an adequate amplitude for the vicinity threshold parameter brings benefices to the understanding of the phenomenon and better results of the recurrence analysis can be acquired.

V. DISCUSSIONS AND CONCLUSIONS

In this work, we have explored how an optimized procedure to obtain the vicinity threshold of recurrence analyses can be used to enhance the sensitivity of recurrence quantifiers to detect nonstationary behavior, as well as to infer coupling between different systems. Making use of two dynamical systems, we have shown that nonstationary behavior imposed by the insertion of small variations of system parameters can be clearly identified using a running windowed recurrence quantifier.

Using the optimized procedure to obtain the recurrence vicinity threshold parameter, we have explored subtle changes occurring in data captured by accelerometer sensors during mice deep sleep periods. Our results have shown that the time interval between two successive arousals shows a common dynamical behavior, namely, the windowed obtained quantifier $\Delta(\varepsilon)$ (the determinism) computed from accelerometer data suffers a progressive increase of amplitude, followed by an abrupt decrease some seconds before the next arousal event. That behavior means that during the slow-wave sleep episode between two consecutive arousals, the determinism increases until it reaches a critical threshold, and then, some seconds before the next arousal, its amplitude starts to drop quickly going to an almost vanishing value. The decrease of the amplitude precedes the arousal itself by some seconds, suggesting that it can be used as a predictor of arousals. The increase of determinism of the accelerometer records during a SWS episode and its abrupt decrease before arousals means that subtle changes in the temporal signal of the accelerometer are occurring, reflecting physiologic changes such as breathing activity movement, heart beating, tremors, or limbic movement. The fact that a maximum of determinism is attained before arousal events suggests that we can use this methodology as a cheap and non-invasive precursor of arousals. In this way, the use of determinism as a tool for arousal predictability could provide a promising technique for sleep apnea diagnostic and treatment, as well as neurodegenerative diseases with sleep disturbances.

Fast Fourier analyses of the A_{cc} signals were computed (i) during sleep periods, when $\Delta(A_{cc})$ signal stays above 75% of its maximum and (ii) some seconds before an arousal be observed, after $\Delta(A_{cc})$ starts to drop and before reaches 25% of its maximum. Such analyses should corroborate our findings about the existence of different patterns in the $\Delta(A_{cc})$ profile. Here, we emphasize that such distinct patterns in $\Delta(A_{cc})$ are captured in real time, without any average over time. Different from the use of the optimized recurrence analysis, the analysis in real time of the signal via fast Fourier of only one event does not bring evidences of changes. Nevertheless, when mean values of normalized Fourier spectra of A_{cc} and H_{pp} signals ($\approx$3 s of time sampling) are captured and integrated for 200 events including data from all 5 individuals, changes in the mean frequency can be observed. Figure 11 depicts results for the mean values of the Fast Fourier Transform for the signals, taking into account all 200 events. Black (green) curves correspond to spectra from A_{cc} (H_{pp}) for time intervals: (a) very before the arousal, in the stationary sleep periods and (b) for the time periods when $\Delta(A_{cc})$ starts to drop (first seconds of gray rectangles in Figs. 7 and 8). Clearly, a higher frequency mode appears during the time interval just before the arousal, distinguishing this part of the sleep from others as predicted by the use of the recurrence analysis. These observations evidence that the time interval corresponding to

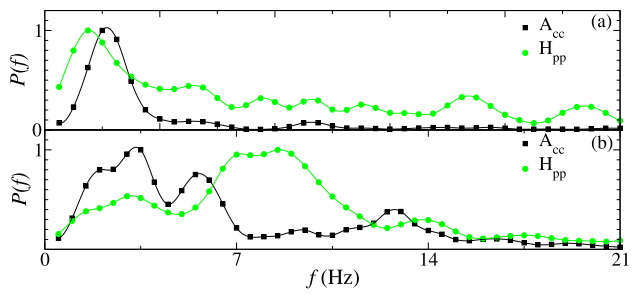

FIG. 11. Mean values of normalized Fourier spectra of A_{cc} and H_{pp} obtained from 200 arousal events for (a) time intervals of stationary sleep, where $\Delta(A_{cc})$ is stable and above 0.8 (on the left of gray rectangles in Figs. 7 and 8). (b) Time intervals just after the stationarity breaking of sleep, where $\Delta(A_{cc})$ starts to drop (first seconds of gray rectangles in Figs. 7 and 8).

some second before an arousal during the deep sleep phase can be in fact a distinct part of the sleep having its own properties.

Since Fast Fourier analysis is not sensitive enough, a large number of events is necessary in order to observe a clear change in the pattern for $P(f)$ for both signals. So, the simultaneously observed changes in both signals $\Delta(A_{cc})$ and $\Delta(H_{pp})$ confirm our finding that recurrence analysis can be very sensitive to detect small changes in time series patterns, allowing the use of a recurrence analysis of only one event to infer the behavior of both curves.

In conclusion, we have proposed a new way to calculate the vicinity threshold parameter in recurrence analysis. A strong point of the methodology is that, considering a time series, the value of the parameter can be automatically determined such that all analyses can be automatically performed.

We have shown how the recurrence quantifier $[\Delta(\varepsilon)]$, subjected to an optimization process for the computation of the vicinity threshold parameter ε, can be used to quantify (non)stationary behaviors of time series as well as to infer coupling between dynamical systems. This study brings the possibility of the use of recurrence analysis to monitor changes in phase/parameter spaces using just collected data, improving the knowledge obtained from other more traditional time series analysis methods. Furthermore recognizing that, in general, systems interact with its ambient and that interactions are unavoidable and results in changes on the system parameter space, the possibility to detect even small changes on this space can be used as a tool to monitor experimental setups.

In our experimental example, a large amount of data collected during sleep periods of mammals (mice) has been studied using recurrence analysis, giving a confident statistics analysis. Results suggest a coupling between two distinct signals, one obtained from an accelerometer attached to the head of the individuals and a second one, collected from deep electrodes surgically implanted into CA_1 area of mice brain area. Our findings show that it is possible to define a clear pattern in the signal obtained by windowed computed recurrence quantifier $\Delta(\varepsilon)$, observed as an accentuated dropping on its amplitude some seconds before any noticeable changes in A_{cc} for more than 85% of analyzed arousal events. This pattern is observed to occur almost synchronized with substantial changes in the hippocampus local field potential signals. This fact brings evidences of a strong correlation between both signals, suggesting a possible cause-effect situation in which a hippocampus activity suffers changes in its activity before the occurrence of a burst motion activity (a visual detectable arousal). This scenario suggests that the brain (specially hippocampus areas) can promote arousals as part of a complex mechanism responsible for sleep regulation. Such data can corroborate the idea that arousals can be considered as part of sleep as already pointed out in Ref. 39.

ACKNOWLEDGMENTS

The authors thank the Instituto Internacional de Neurociências Edmond and Lily Safra (IINN-ELS) for allowing data collection and Sidarta T. G. Ribeiro and Miguel Nicolelis for the kind support. This work received financial support from CNPq (Grant Nos. 552148/2011-3 and 470716/2013-4), CAPES (Grant Nos. 88881.119252/2016-01 and BEX: 11264/13-6), and FINEP (CT-Infra, UFPR) (Brazilian agencies). Simulations were performed at LCPAD/UFPR.

[1]P. C. D. Milly, J. Betancourt, M. Falkenmark, R. M. Hirsch, Z. W. Kundzewicz, D. P. Lettenmaier, and R. J. Stouffer, "Stationarity is dead: Whither water management?," Science **319**(5863), 573–574 (2008).
[2]C. Rieke, K. Sternickel, R. G. Andrzejak, C. E. Elger, P. David, and K. Lehnertz, "Measuring nonstationarity by analyzing the loss of recurrence in dynamical systems," Phys. Rev. Lett. **88**(24), 244102 (2002).
[3]G. E. P. Box, G. M. Jenkins, G. C. Reinsel, and G. M. Ljung, *Time Series Analysis: Forecasting and Control* (John Wiley & Sons, 2015).
[4]*Nonlinear Analysis of Physiological Data*, 1st ed., edited by H. Kantz, J. Kurths, and G. Mayer-Kress (Springer-Verlag, Heidelberg, Germany, 1998).
[5]P. Bernaola-Galván, P. Ch. Ivanov, L. A. Nunes Amaral, and H. E. Stanley, "Scale invariance in the nonstationarity of human heart rate," Phys. Rev. Lett. **87**, 168105 (2001).
[6]P. M. Robinson, *Time Series with Long Memory* (Advanced Texts in Econometrics, 2003).
[7]Y. Ashkenazy, P. Ch. Ivanov, S. Havlin, C.-K. Peng, A. L. Goldberger, and H. E. Stanley, "Magnitude and sign correlations in heartbeat fluctuations," Phys. Rev. Lett. **86**, 1900–1903 (2001).
[8]L. Xu, Z. Chen, K. Hu, H. E. Stanley, and P. Ch. Ivanov, "Spurious detection of phase synchronization in coupled nonlinear oscillators," Phys. Rev. E **73**, 065201 (2006).
[9]P. Bernaola-Galván, J. L. Oliver, M. Hackenberg, A. V. Coronado, P. Ch. Ivanov, and P. Carpena, "Segmentation of time series with long-range fractal correlations," Eur. Phys. J. B **85**(6), 211 (2012).
[10]M. G. Rosenblum, A. S. Pikovsky, and J. Kurths, "Phase synchronization of chaotic oscillators," Phys. Rev. Lett. **76**, 1804–1807 (1996).
[11]M. G. Rosenblum, A. S. Pikovsky, and J. Kurths, "From phase to lag synchronization in coupled chaotic oscillators," Phys. Rev. Lett. **78**, 4193–4196 (1997).
[12]Z. Chen, K. Hu, H. E. Stanley, V. Novak, and P. Ch. Ivanov, "Cross-correlation of instantaneous phase increments in pressure-flow fluctuations: Applications to cerebral autoregulation," Phys. Rev. E **73**, 031915 (2006).
[13]T. Stankovski, A. Duggento, P. V. E. McClintock, and A. Stefanovska, "Inference of time-evolving coupled dynamical systems in the presence of noise," Phys. Rev. Lett. **109**, 024101 (2012).
[14]A. Bashan, R. P. Bartsch, J. W. Kantelhardt, S. Havlin, and P. Ch. Ivanov, "Network physiology reveals relations between network topology and physiological function," Nat. Commun. **3**, 702 (2012).
[15]R. P. Bartsch, K. K. L. Liu, A. Bashan, and P. Ch. Ivanov, "Network physiology: How organ systems dynamically interact," PLoS ONE **10**(11), 1–36 (2015).
[16]N. Marwan, M. C. Romano, M. Thiel, and J. Kurths, "Recurrence plots for the analysis of complex systems," Phys. Rep. **438**(5-6), 237–329 (2007).
[17]E. G. Souza, R. L. Viana, and S. R. Lopes, "Using recurrences to characterize the hyperchaos-chaos transition," Phys. Rev. E **78**, 066206 (2008).
[18]R. C. Budzinski, B. R. R. Boaretto, T. L. Prado, and S. R. Lopes, "Detection of nonstationary transition to synchronized states of a neural network using recurrence analyses," Phys. Rev. E **96**(1), 012320 (2017).
[19]D. B. Vasconcelos, S. R. Lopes, R. L. Viana, and J. Kurths, "Spatial recurrence plots," Phys. Rev. E **73**, 056207 (2006).
[20]T. L. Prado, P. P. Galuzio, S. R. Lopes, and R. L. Viana, "Spatial recurrence analysis: A sensitive and fast detection tool in digital mammography," Chaos **24**(1), 013106 (2014).
[21]J. P. Zbilut and C. L. Webber, "Recurrence quantification analysis: Introduction and historical context," Int. J. Bifurcat. Chaos **17**(10), 3477–3481 (2007).
[22]G. Z. dos Santos Lima, S. R. Lopes, T. L. Prado, B. Lobao-Soares, G. C. do Nascimento, J. Fontenele-Araujo, and G. Corso, "Predictability of arousal in mouse slow wave sleep by accelerometer data," PloS ONE **12**(5), e0176761 (2017).
[23]H. Poincaré, "Sur la probleme des trois corps et les équations de la dynamique," Acta Math. **13**(1), 1–271 (1890).
[24]J.-P. Eckmann, S. O. Kamphorst, and D. Ruelle, "Recurrence plots of dynamical systems," Europhys. Lett. **4**(9), 973 (1987).

[25]J. P. Zbilut and C. L. Webber, "Embeddings and delays as derived from quantification of recurrence plots," Phys. Lett. A **171**(3), 199–203 (1992).
[26]J. P. Zbilut, J. M. Zaldivar-Comenges, and F. Strozzi, "Recurrence quantification based Liapunov exponents for monitoring divergence in experimental data," Phys. Lett. A **297**(3-4), 173–181 (2002).
[27]J. B. Gao, "Recurrence time statistics for chaotic systems and their applications," Phys. Rev. Lett. **83**(16), 3178 (1999).
[28]C. Letellier, "Estimating the shannon entropy: Recurrence plots versus symbolic dynamics," Phys. Rev. Lett. **96**(25), 254102 (2006).
[29]M. Thiel, M. C. Romano, J. Kurths, R. Meucci, E. Allaria, and F. T. Arecchi, "Influence of observational noise on the recurrence quantification analysis," Physica D **171**(3), 138–152 (2002).
[30]R. Manuca and R. Savit, "Stationarity and nonstationarity in time series analysis," Physica D **99**(2), 134–161 (1996).
[31]M. B. Kennel, "Statistical test for dynamical nonstationarity in observed time-series data," Phys. Rev. E **56**(1), 316 (1997).
[32]Y. Chen and H. Yang, "Multiscale recurrence analysis of long-term nonlinear and nonstationary time series," Chaos Solitons Fractals **45**(7), 978–987 (2012).
[33]J. B. Gao, "Detecting nonstationarity and state transitions in a time series," Phys. Rev. E **63**(6), 066202 (2001).
[34]L. L. Trulla, A. Giuliani, J. P. Zbilut, and C. L. Webber, "Recurrence quantification analysis of the logistic equation with transients," Phys. Lett. A **223**(4), 255–260 (1996).
[35]Y. Liu, M. Kankaanpää, J. P Zbilut, and C. L Webber, "EMG recurrence quantifications in dynamic exercise," Biol. Cybern. **90**(5), 337–348 (2004).
[36]N. Marwan and A. Meinke, "Extended recurrence plot analysis and its application to erp data," Int. J. Bifurcat. Chaos **14**(02), 761–771 (2004).
[37]L. M. Pecora, T. L. Carroll, G. A. Johnson, D. J. Mar, and J. F. Heagy, "Fundamentals of synchronization in chaotic systems, concepts, and applications," Chaos **7**(4), 520–543 (1997).
[38]G. Z. dos Santos Lima, B. Lobão-Soares, G. C. do Nascimento, A. S. C. França, L. Muratori, S. Ribeiro, and G. Corso, "Mouse activity across time scales: Fractal scenarios," PLoS ONE **9**(10), 1–12 (2014).
[39]P. Halász, M. Terzano, L. Parrino, and R. Bódizs, "The nature of arousal in sleep," J. Sleep Res. **13**(1), 1–23 (2004).
[40]J. Trinder, N. Allen, J. Kleiman, V. Kralevski, D. Kleverlaan, K. Anson, and Y. Kim, "On the nature of cardiovascular activation at an arousal from sleep," Sleep **26**(5), 543–551 (2003).